Temperature-dependent EXAFS analysis of embedded Pt nanocrystals

2009 J. Phys.: Condens. Matter 21 155302

(http://iopscience.iop.org/0953-8984/21/15/155302)

J. Phys.: Condens. Matter **21** (2009) 155302 (6pp) doi:10.1088/0953-8984/21/15/155302

Temperature-dependent EXAFS analysis of embedded Pt nanocrystals

R Giulian[1], L L Araujo[1], P Kluth[1], D J Sprouster[1], C S Schnohr[1], G J Foran[2] and M C Ridgway[1]

[1] Department of Electronic Materials Engineering, Research School of Physics and Engineering, Australian National University, Canberra, ACT 0200, Australia
[2] Australian Nuclear Science and Technology Organisation, Menai, NSW 2234, Australia

E-mail: raq109@rsphysse.anu.edu.au

Received 29 October 2008, in final form 9 February 2009
Published 17 March 2009
Online at stacks.iop.org/JPhysCM/21/155302

Abstract

The vibrational and thermal properties of embedded Pt nanocrystals (NCs) have been investigated with temperature-dependent extended x-ray absorption fine structure (EXAFS) spectroscopy. NCs of diameter 1.8–7.4 nm produced by ion implantation in amorphous SiO_2 were analysed over the temperature range 20–295 K. An increase in Einstein temperature (∼194 K) relative to that of a Pt standard (∼179 K) was evident for the smallest NCs while those larger than ∼2.0 nm exhibited values comparable to bulk material. Similarly, the thermal expansion of interatomic distances was lowest for small NCs. While the amorphous SiO_2 matrix restricted the thermal expansion of interatomic distances, it did not have a significant influence on the mean vibrational frequency of embedded Pt NCs. Instead, the latter was governed by finite-size effects or, specifically, capillary pressure.

(Some figures in this article are in colour only in the electronic version)

1. Introduction

Nanocrystals (NCs) are promising building blocks for novel technological applications in the fields of catalysis [1], optics [2], medicine [3], etc [4]. In particular, the enhanced catalytic activity of Pt NCs plays an important role in the reduction of pollutant gases exhausted from automobiles [1, 5]. Finite-size effects yield the technologically relevant differences in NC and bulk behaviour and govern the NC structural [6–8] and vibrational properties [9–15]. Such properties have been previously examined for free-standing and functionalized Pt NCs [11, 14, 15]. For this experiment, we examine Pt NCs embedded in amorphous SiO_2 (a-SiO_2) as most appropriate for photonic applications. We utilize a broad range of NC sizes and an increased number of temperature points with the aim of establishing the relative influences of finite-size effects, the surrounding environment, H chemisorption and preparation method. We are then better able to compare new and previously published results to aid in the more rapid integration of Pt NCs in novel device applications.

The use of extended x-ray absorption fine structure (EXAFS) spectroscopy as a probe of vibrational and thermal properties has been under constant development, as evident in the representative works comprising [9, 12, 16–27]. Recently, Fornasini and co-workers [16, 17] have highlighted the differences between parameters measured by EXAFS and x-ray diffraction. From temperature-dependent EXAFS measurements, one can obtain information on the variation of the mean value (interatomic distance), variance (Debye–Waller factor) and asymmetry (third cumulant) of the first-shell interatomic distance distribution over the given temperature range. The Einstein temperature, the thermal and structural contributions to total disorder, the anharmonicity of the effective pair potential and the linear thermal expansion coefficient can all be extracted from the experimental data via the appropriate combination of a correlated Debye or Einstein model and thermodynamic perturbation theory [16–19]. We have previously demonstrated that this approach can be readily extended to the study of embedded metal and semiconductor NCs [9, 27] and now apply this method to Pt NCs produced by ion implantation in a-SiO_2 to study their vibrational and thermal properties as a function of NC size.

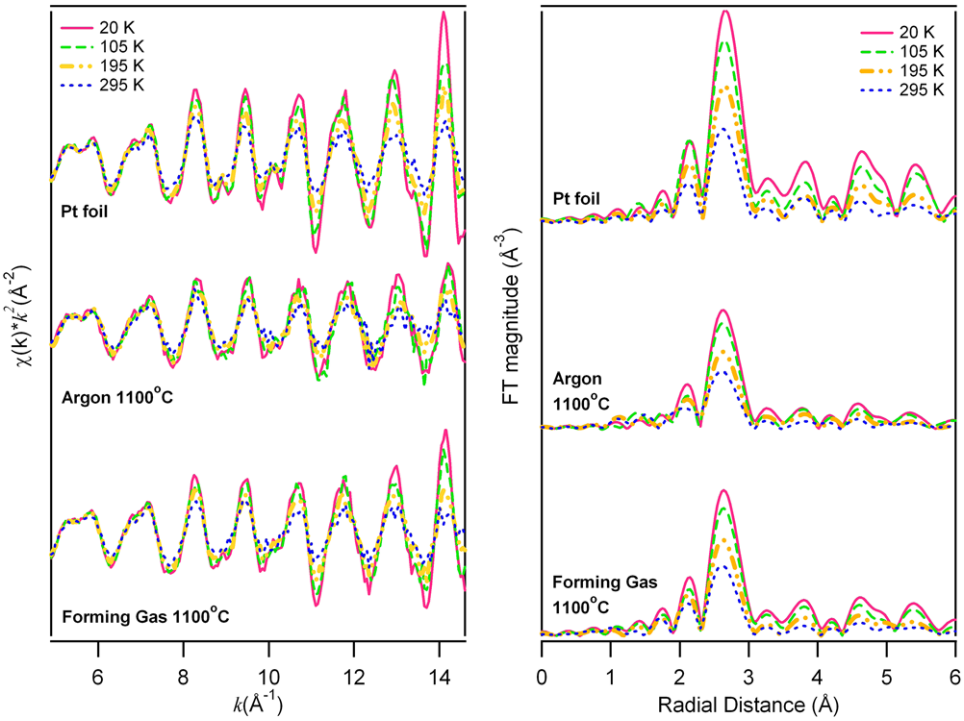

Figure 1. k^2-weighted (left) and Fourier-transformed (non-phase-corrected) EXAFS spectra (right). Measurement temperatures are specified in the legend.

Table 1. Values of mean NC diameter (D_{mean}) estimated from SAXS measurements ([28]), the CN determined at 20 K, the structural contribution to total disorder ($\sigma^2_{\mathrm{static}}$), the Einstein temperature (Θ_{E}) and the thermal expansion of interatomic distances (ΔR) between 20 and 295 K obtained from EXAFS analysis.

Sample		D_{mean} (nm)	CN (atoms)	$\sigma^2_{\mathrm{static}}$ (Å^2)	Θ_{E} (K)	ΔR (Å)
Pt foil		—	12	0.0003 ± 0.0001	179 ± 2	0.014 ± 0.001
Ar	1200 °C	4.0 ± 0.6	11.5 ± 0.7	0.0007 ± 0.0001	178 ± 2	0.013 ± 0.001
	1100 °C	2.8 ± 0.4	9.8 ± 0.5	0.0019 ± 0.0001	177 ± 3	0.006 ± 0.001
	1000 °C	1.8 ± 0.2	8.8 ± 0.7	0.0031 ± 0.0001	194 ± 5	0.005 ± 0.001
FG	1200 °C	7.4 ± 1.3	10.1 ± 1.0	0.0012 ± 0.0001	178 ± 2	0.016 ± 0.002
	1100 °C	3.5 ± 0.5	10.4 ± 0.5	0.0013 ± 0.0001	182 ± 1	0.010 ± 0.001
	1000 °C	2.7 ± 0.4	9.1 ± 0.5	0.0015 ± 0.0001	183 ± 1	0.006 ± 0.001

2. Experimental details

Amorphous SiO_2 layers (2 μm thick) thermally grown on Si substrates were implanted at liquid N_2 temperature with 4.5 MeV Pt ions for a total fluence of 1×10^{17} cm^{-2}. Samples were then annealed in either Ar or forming gas (FG, 95% $N_2 + 5\%$ H_2) for 1 h at temperatures of 1000–1200 °C. The mean NC diameter was determined from small-angle x-ray scattering (SAXS) and transmission electron microscopy (TEM) measurements [28] and varied from 1.8 to 7.4 nm, as listed in table 1 as a function of annealing temperature and ambient.

Temperature-dependent EXAFS measurements were performed at beamline 20-B of the Photon Factory, Japan, in fluorescence mode at the Pt L_3 edge (11 564 eV). The temperature was controlled to ± 1 K and measurements were performed at eight temperatures in the range 20–295 K. Spectra were collected with a 6×6 pixel array Ge detector and the Si(111) monochromator was detuned by 50% for harmonic rejection. For energy calibration, a bulk Pt sample was measured simultaneously in transmission mode. NC samples were prepared by removing the Si substrate from the SiO_2 layer using a combination of mechanical grinding and selective wet chemical etching in a KOH solution [6]. A 200 nm Pt foil was used as a bulk standard for the fluorescence measurements.

EXAFS data were analysed using the ATHENA [29] and ARTEMIS [29] programs, interfaces for the IFEFFIT [30] and FEFF [24] codes. After background removal, the spectra were Fourier-transformed over a photoelectron wavenumber (k) range of 4.9–14.6 Å^{-1}. Representative spectra are shown in figure 1 within which scattering from the first four nearest-neighbour (NN) shells is apparent. Clearly the amplitude decreases as the measurement temperature increases or, equivalently, as thermal disorder becomes more significant. Comparing NC and bulk sample spectra at a given measurement temperature, the decreased amplitude of the former is the result of finite-size effects, specifically the

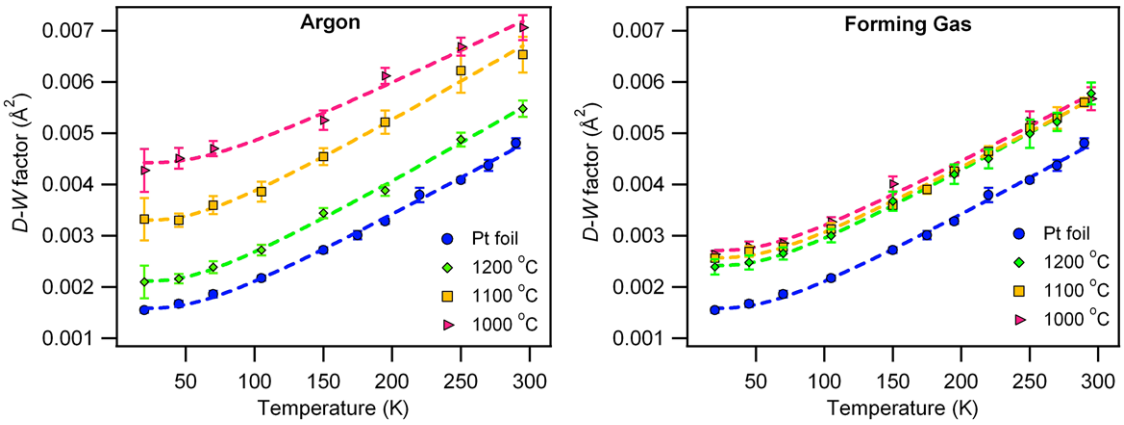

Figure 2. D–W factor as a function of measurement temperature. Dashed lines are fits to the experimental values using (1).

reduced average coordination number and enhanced structural disorder associated with the non-negligible surface-to-volume ratio in the NCs. For a fixed measurement temperature of 20 K, we have discussed in detail the variation of these two structural parameters as a function of NC size in [28]. For the present paper, we now focus on measurement-temperature-dependent properties.

3. Data analysis

Structural parameters were extracted from the first NN shell, the latter isolated by inverse Fourier-transforming over a non-phase-corrected radial distance range of 1.7–3.1 Å. Theoretical standards generated by the FEFF8 code [24] were fitted to the experimental spectra. The amplitude reduction factor (S_0^2) and energy shift parameter (ΔE_0) were determined from the Pt foil (0.84 ± 0.06 and 14.9 ± 0.9 eV, respectively) and kept constant thereafter. For the NC samples, the coordination number (CN) was determined from the lowest-temperature measurement and then fixed (values are presented in table 1), while that for the Pt foil was set equal to 12 atoms.

The mean interatomic distance (R), variance (Debye–Waller (D–W) factor) and asymmetry (third cumulant (C_3)) of the first NN shell were first determined from individual fits to each spectrum with the coordination number fixed as described above. (Note that analysis with IFEFFIT yields values for R directly without the need for a photoelectron mean-free-path correction (as required with a ratio-method-type approach).) Figure 2 shows the D–W factor (σ^2) as a function of the measurement temperature (T) and fitted with a correlated Einstein model [9, 23] given by

$$\sigma^2 = \frac{\hbar^2}{2\mu k_B \Theta_E} \coth\left(\frac{\Theta_E}{2T}\right) + \sigma^2_{static} \qquad (1)$$

where $\hbar$ is Planck's constant divided by 2π, μ is the reduced mass for the scatterer–absorber pair, k_B is Boltzmann's constant and Θ_E is the Einstein temperature. The first and second terms of (1) represent, respectively, the thermal and structural contributions (σ^2_{static}) to the total disorder. The Einstein frequency ω_E is calculable from $\Theta_E = \hbar\omega_E/k_B$ and, as Vaccari and Fornasini note, represents both the effective vibrational frequency of the absorber–scatterer pair (thus relating to the force constant of the interatomic bond) and, approximately, the centroid of the distribution of normal mode frequencies [23].

Having determined Θ_E from the amplitude-dependent parameters, correlation between the phase-dependent parameters R and C_3 was then reduced by restraining the latter to the relation derived from the anharmonic one-dimensional effective potential given in [9, 19]:

$$C_3(T) = \frac{k_3 k_B^2 \Theta_E}{2k_{eff}^3} \frac{1 + 10z + z^2}{(1-z)^2} + C_{3static}, \qquad (2)$$

where $z \equiv \exp(-\Theta_E/T)$, k_3 is the cubic anharmonic force constant, $C_{3static}$ is the asymmetry from structural contributions and k_{eff} is the effective harmonic spring constant defined as $k_{eff} = \mu k_B^2 \hbar^2 \Theta_E^2$. For a given sample, the datasets over all temperatures were then refitted simultaneously with S_0^2, ΔE_0, CN and σ^2 fixed as described above, C_3 restrained using (2) and R floated freely.

4. Results and discussion

4.1. Debye–Waller factors and Einstein temperatures

The general increase in D–W factor with increasing measurement temperature is readily apparent in figure 2 for all samples and, as before, is the result of increasing thermal disorder. Fitting with (1) enables us to separate the structural and thermal contributions to the total disorder and determine the Einstein temperature. Values are listed in table 1 as a function of annealing temperature, annealing ambient and mean NC diameter. For the Pt foil, our results agree well with those of Kang *et al* [15]. For the Pt NCs, figure 3 demonstrates that structural disorder increases with a decrease in NC size or increase in surface-to-volume ratio as the relaxation of under-coordinated surface atoms results in a wider distribution of interatomic distances [14, 28, 31]. Similar values have been reported for Pt [11, 14, 15, 31] and other metallic NCs [10, 12, 16]. Note that samples annealed in FG at 1200 °C (7.4 nm) surprisingly exhibit greater structural disorder than those annealed in Ar at the same temperature (4.0 nm),

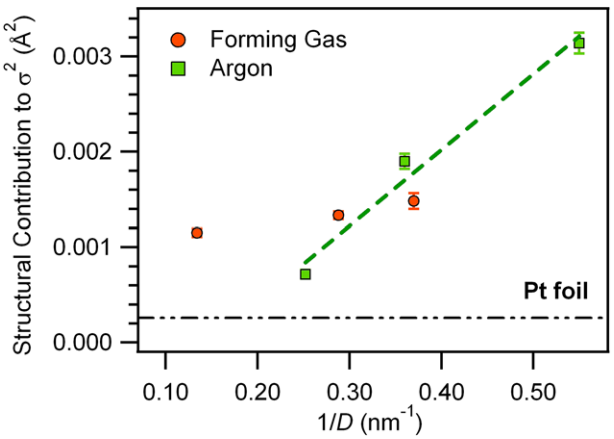

Figure 3. Structural contribution to σ^2 as a function of inverse NC diameter.

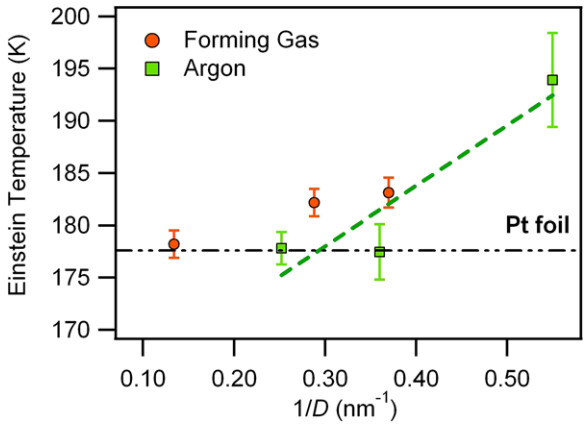

Figure 4. Einstein temperature as a function of inverse NC diameter.

inconsistent with a surface-to-volume argument. Instead, this result is due to H chemisorption in Pt NCs annealed in FG at temperatures of 1100 and 1200 °C which yields an increase in both interatomic distance and structural disorder [28].

With reference to table 1, the Einstein temperature of the smaller NCs ($\lesssim$3 nm) increases relative to that of the Pt foil, indicative of stiffer bonding. Higher Θ_E values have also been reported for free-standing and/or functionalized Pt NCs of comparable size [11, 14, 15]. The larger Pt NCs (including those with chemisorbed H) rapidly converge to bulk-like values, again consistent with previous observations for free-standing Pt NCs [14]. Neither the a-SiO_2 matrix nor chemisorbed H significantly influence the Einstein temperature of the Pt NCs examined in this report. The higher Θ_E values observed for the smaller NCs are due to capillary pressure which shifts the vibrational density of states (VDOS) upwards [32, 33] but, as described below, reduces the interatomic distance. Capillary pressure is the result of surface curvature and, according to the Kelvin equation, varies inversely with NC diameter [32, 33]. Figure 4 shows that Θ_E scales with inverse NC diameter and thus capillary pressure. Reports for other metal NCs (∼3 nm) embedded in a-SiO_2 indicate the Einstein temperature may be either lower (Cu [27] and Sn [34]) or similar (Au [27]) to that of bulk standards. The former was attributed to loosely bound surface/interfacial atoms shifting the VDOS downwards to a greater extent than the counterbalancing effect of capillary pressure. Clearly an intricate interplay between finite-size effects (capillary pressure and surface disorder), surface functionalization (including H chemisorption) and the embedding matrix must govern the vibrational properties of NCs. From the results presented in this report, we conclude that finite-size effects, specifically capillary pressure, are the dominant influence for Pt NCs.

4.2. Interatomic distances and third cumulants

Values for R and C_3 are plotted in figure 5 as a function of the measurement temperature. The pressure exerted on the NC core as a result of surface curvature yields, in general, a reduced interatomic distance relative to that of the Pt foil, consistent with previous reports for other metals [10, 14, 31]. As the NCs increase in size, the capillary pressure decreases in magnitude and, accordingly, R approaches the bulk value. Samples with chemisorbed H (those annealed in FG at 1100 and 1200 °C) remain the exception with R values comparable to or greater than the bulk value. This difference increases as a function of H content or, equivalently, the annealing temperature in FG.

From figure 5, the interatomic distances clearly increase with measurement temperature. The linear thermal expansion ($\Delta R = R_{295\ K} - R_{20\ K}$) is presented in figure 6 as a function of inverse NC diameter, with values listed in table 1. Excluding the sample with appreciable chemisorbed H, NCs exhibit less thermal expansion than the Pt foil and the difference becomes more pronounced as the NC size decreases. Comparing our results with those for free-standing Pt NCs [14] (where NC $>$ 2.4 nm show positive thermal expansion similar to that of the bulk), the a-SiO_2 matrix appears to restrict the thermal expansion of embedded Pt NCs consistent with the negative thermal expansion coefficient of a-SiO_2 below 180 K and a very low yet positive coefficient above this temperature [35, 36]. Similar results have been reported for Ge NCs [37]. Other reports include nil thermal expansion for functionalized Pt NCs [11] and a negative thermal expansion for Pt NCs supported on Al_2O_3 [15], the latter attributed to Pt–Al_2O_3 interaction. Using both EXAFS and x-ray diffraction [38, 39], an unusual crossover from positive to negative thermal expansion has been observed in Au NCs at ∼125 K as consistent with a NC-size-dependent contribution of electronic excitations to the total energy of the system [39]. Such results illustrate that finite-size effects, surface functionalization and the surrounding environment can also influence the thermal properties of NCs.

For all samples, figure 5 also demonstrates the asymmetry of the interatomic distance distribution increases with an increase in measurement temperature, as expected from the anharmonicity of the effective potential. The spectra are offset vertically as a result of differences in the structural contribution to C_3 and generally this component increases with a decrease in NC size, in good agreement with results for supported Pt NCs [31].

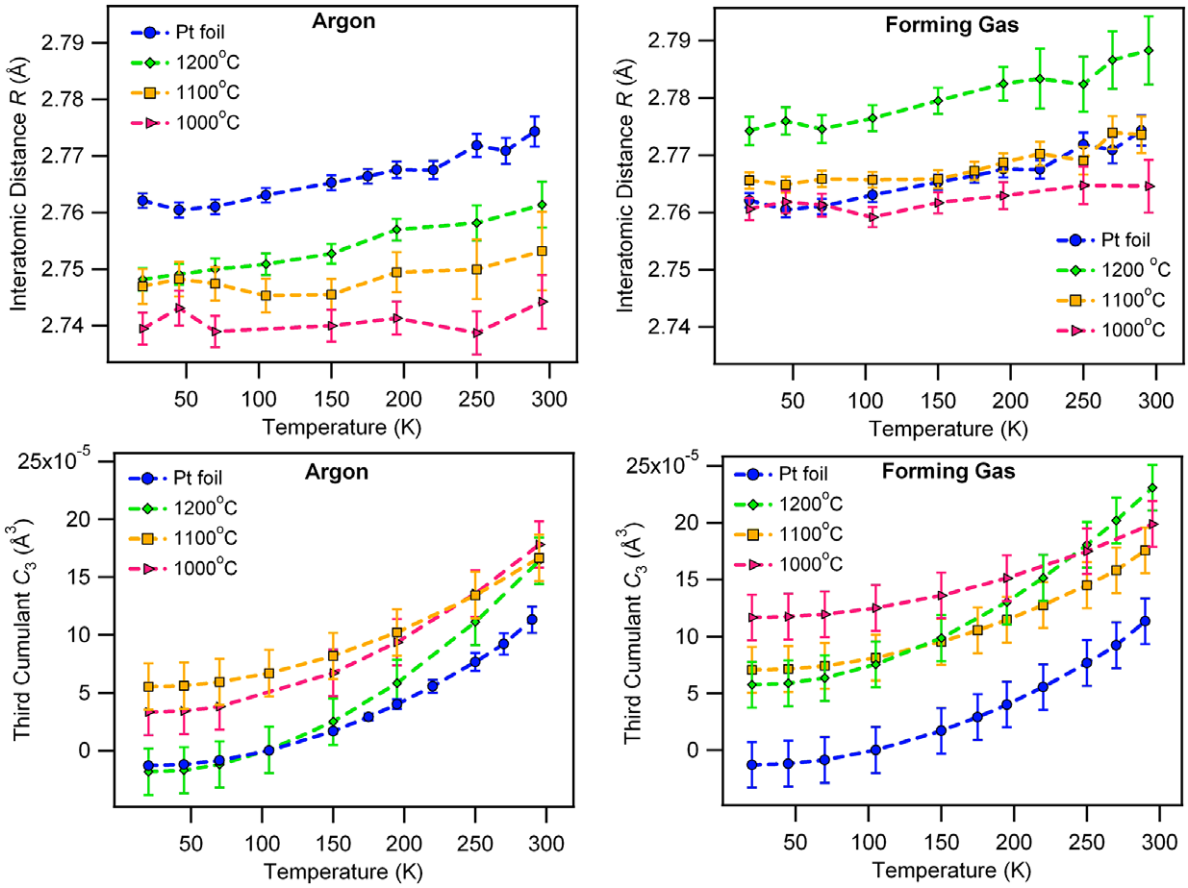

Figure 5. Interatomic distance R (top) and asymmetry C_3 (bottom) as a function of measurement temperature.

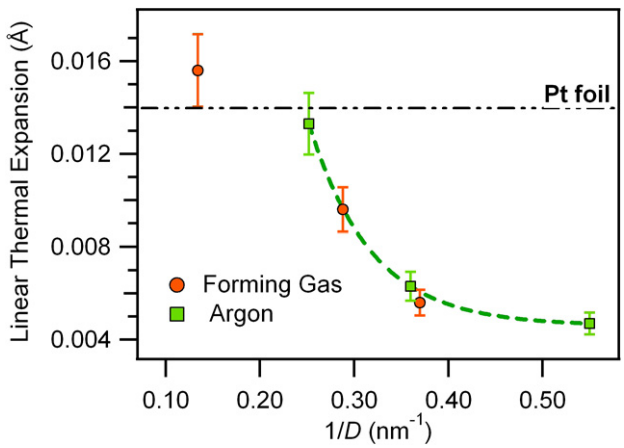

Figure 6. Linear thermal expansion ($\Delta R = R_{295\ \mathrm{K}} - R_{20\ \mathrm{K}}$) as a function of inverse NC diameter. The dashed line is a guide to the eye.

5. Conclusions

In summary, the vibrational and thermal properties of Pt NCs embedded in a-SiO_2 have been characterized using temperature-dependent EXAFS analysis. The interatomic distance, structural and thermal disorder and asymmetry have been determined as a function of measurement temperature and NC size. Relative to bulk values, the structural disorder and mean vibrational frequency increased as the NC diameter decreased. Pt NCs thus exhibit stiffer bonding compared to their bulk counterparts. The vibrational properties of embedded Pt NCs are not significantly influenced by the a-SiO_2 matrix or H chemisorption. The constraint imposed by the matrix can, however, reduce the thermal expansion of embedded Pt NCs.

Acknowledgment

The authors thank the Australian Research Council and Australian Synchrotron Research Programme for financial support.

References

[1] Bell A T 2003 *Science* **299** 1688
[2] Pavesi L, Dal Negro L, Mazzoleni C, Franzo G and Priolo F 2000 *Nature* **408** 440
[3] El-Sayed I H, Huang X and El-Sayed M A 2006 *Cancer Lett.* **239** 129
[4] Roduner E 2006 *Chem. Soc. Rev.* **35** 583
[5] Narayanan R and El-Sayed M A 2004 *Nano Lett.* **4** 1343
[6] Cheung A, Azevedo G d M, Glover C J, Llewellyn D J, Elliman R G, Foran G J and Ridgway M C 2004 *Appl. Phys. Lett.* **84** 278

[7] Johannessen B, Kluth P, Glover C J, Azevedo G d M, Llewellyn D J, Foran G J and Ridgway M C 2005 *J. Appl. Phys.* **98** 024307
[8] Kluth P, Johannessen B, Giraud V, Cheung A, Glover C J, Azevedo G d M, Foran G J and Ridgway M C 2004 *Appl. Phys. Lett.* **85** 3561
[9] Araujo L L, Kluth P, Azevedo G d M and Ridgway M C 2006 *Phys. Rev.* B **74** 184102
[10] Johannessen B, Kluth P, Giulian R, Araujo L L, Llewellyn D J, Foran G J, Cookson D J and Ridgway M C 2007 *Nucl. Instrum. Methods* B **257** 37
[11] Giovanetti L J, Ramallo-Lopez J M, Requejo F G, Garcia-Gutierrez D I, Jose-Yacaman M and Craievich A F 2007 *J. Phys. Chem.* C **111** 7599
[12] Gilbert B, Huang F, Zhang H Z, Waychunas G A and Banfield J F 2004 *Science* **305** 651
[13] Dubiel M, Brunsch S and Troger L 2000 *J. Phys.: Condens. Matter* **12** 4775
[14] Frenkel A I, Hills C W and Nuzzo R G 2001 *J. Phys. Chem.* B **105** 12689
[15] Kang J H, Menard L D, Nuzzo R G and Frenkel A I 2006 *J. Am. Chem. Soc.* **128** 12068
[16] Fornasini P, Beccara S A, Dalba G, Grisenti R, Sanson A, Vaccari M and Rocca F 2004 *Phys. Rev.* B **70** 174301
[17] Fornasini P 2007 *AIP Conf. Proc.* **882** 94
[18] Troger L, Yokoyama T, Arvanitis D, Lederer T, Tischer M and Baberschke K 1994 *Phys. Rev.* B **49** 888
[19] Frenkel A I and Rehr J J 1993 *Phys. Rev.* B **48** 585
[20] Dalba G, Fornasini P, Grisenti R and Purans J 1999 *Phys. Rev. Lett.* **82** 4240
[21] Knapp G S, Pan H K and Tranquada J M 1985 *Phys. Rev.* B **32** 2006
[22] Van Hung N, Duc N B and Frahm R R 2003 *J. Phys. Soc. Japan* **72** 1254
[23] Vaccari M and Fornasini P 2006 *J. Synchrotron. Radiat.* **13** 321
[24] Rehr J J and Albers R C 2000 *Rev. Mod. Phys.* **72** 621
[25] Sevillano E, Meuth H and Rehr J J 1979 *Phys. Rev.* B **20** 4908
[26] Stern E A, Bunker B A and Heald S M 1980 *Phys. Rev.* B **21** 5521
[27] Kluth P, Johannessen B, Araujo L L and Ridgway M C 2007 *AIP Conf. Proc.* **882** 731
[28] Giulian R, Araujo L L, Kluth P, Sprouster D J, Schnohr C S, Johannessen B, Foran G J and Ridgway M C 2009 *J. Appl. Phys.* **105** 044303
[29] Ravel B and Newville M 2005 *J. Synchrotron Radiat.* **12** 537
[30] Newville M 2001 *J. Synchrotron Radiat.* **8** 322
[31] Witkowska A, Di Cicco A and Principi E 2007 *Phys. Rev.* B **76** 104110
[32] Meyer R, Lewis L J, Prakash S and Entel P 2003 *Phys. Rev.* B **68**
[33] Meyer R, Prakash S and Entel P 2002 *Phase Transit.* **75** 51
[34] Koops G E J, Pattyn H, Vantomme A, Nauwelaerts S and Venegas R 2004 *Phys. Rev.* B **70** 235410
[35] White G K 1973 *J. Phys. D: Appl. Phys.* **6** 2070
[36] Gaskell P H 1966 *Trans. Faraday Soc.* **62** 1505
[37] Araujo L L, Giulian R, Sprouster D J, Schnohr C S, Llewellyn D J, Kluth P, Cookson D J, Foran G J and Ridgway M C 2008 *Phys. Rev.* B **78** 094112
[38] Comaschi T, Balerna A and Mobilio S 2008 *Phys. Rev.* B **77**
[39] Li W H, Wu S Y, Yang C C, Lai S K, Lee K C, Huang H â L and Yang H â D 2002 *Phys. Rev. Lett.* **89** 135504